Research Article

Senthilkumar Palanisamy*, Kalaivani Subramanian, Lerince Godrina Bennet, Janani Ambrose, Aganiya Gopalakrishnan, Sudhagar Babu, Ranjithkumar Rajamani, Niraj Kumar Jha, Soumya Pandit, Sachin Kumar Singh, Kamal Dua, and Piyush Kumar Gupta*

Synthesis and characterization of PCU@C-Ag/AgCl nanoparticles as an antimicrobial material for respiratory tract infection

Abstract: The pregnant cow urine (PCU) is an active source of antimicrobial agents that is used for fabricating chitosan coated Ag/AgCl nanoparticles (NPs) in the present study. These PCU@C-Ag/AgCl NPs were physicochemically characterized and evaluated for antimicrobial activity against selected respiratory tract infection (RTI) pathogens. The absorption band around 420 nm in UV-Visible spectrum indicated the presence of Ag NPs. The spherical shape of NPs was observed using TEM. Also, the crystalline structure was confirmed using the XRD pattern. The PCU@C-Ag/AgCl NPs showed strong antimicrobial activity against all tested RTI pathogens. In addition, FESEM analysis showed morphological changes in RTI bacterial pathogens. Thereby, PCU@C-Ag/AgCl NPs may be used as an antimicrobial material to treat RTIs in near future at clinical level.
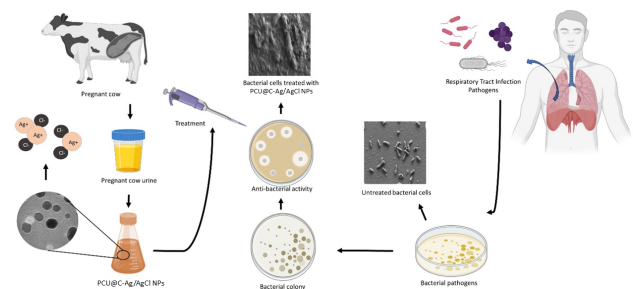
Graphical abstract

1 Introduction

Respiratory Tract Infections (RTIs) are the widest spread and serious infections, accounting for over 65 million people have infected and 3 million deaths globally each year making it to the third leading cause of death worldwide [1]. RTIs include several acute or chronic diseases caused by variety of microorganisms especially both Gram-negative and Gram-positive bacteria like *Pseudomonas aeruginosa, Streptococcus mutans, Klebsiella pneumoniae, Salmonella enteritidis, Haemophilus influenzae, H. parainfluenzae, Seretia marcescens, Enterobacter spp., Acinetobacter spp.,* and

*Corresponding Author: Senthilkumar Palanisamy: Department of Biotechnology, Nehru Arts and Science College, Coimbatore – 641 105, Tamil Nadu, India; Email: senthilkumar1185@gmail.com
*Corresponding Author: Piyush Kumar Gupta: Department of Life Sciences, School of Basic Sciences and Research (SBSR), Sharda University, Knowledge Park III, Greater Noida – 201310, Uttar Pradesh, India; Email: dr.piyushkgupta@gmail.com, piyush.kumar1@sharda.ac.in
Kalaivani Subramanian, Lerince Godrina Bennet, Janani Ambrose, Aganiya Gopalakrishnan: Department of Biotechnology, Kongunadu Arts and Science College, Coimbatore – 641029, Tamil Nadu, India
Sudhagar Babu: Structural Biology Laboratory, Department of Biophysics, National Institute of Mental Health and Neurosciences (NIMHANS), Bangalore – 560030, Karnataka, India
Ranjithkumar Rajamani: Viyen Biotech LLP, Coimbatore – 641031, Tamil Nadu, India

Niraj Kumar Jha: Department of Biotechnology, School of Engineering and Technology (SET), Sharda University, Knowledge Park III, Greater Noida – 201310, Uttar Pradesh, India
Soumya Pandit: Department of Life Sciences, School of Basic Sciences and Research (SBSR), Sharda University, Knowledge Park III, Greater Noida – 201310, Uttar Pradesh, India
Sachin Kumar Singh: School of Pharmaceutical Sciences, Lovely Professional University, Phagwara – 144411, Punjab, India
Kamal Dua: Discipline of Pharmacy, Graduate School of Health, University of Technology Sydney, NSW 2007, Australia; Faculty of Health, Australian Research Centre in Complementary and Integrative Medicine, University of Technology Sydney, Ultimo, 2007 New South Wales, Australia

Moraxella catarrhalis etc. [2]. These pathogenic bacteria frequently cause RTIs in humans and lead to the formation of biofilms on bacterial surface. These biofilms have been known to develop the multidrug resistance condition in bacteria against different antibiotics [3]. After the formation of biofilms, bacteria can be up to 1,000-folds more resistant to antibiotics than those in a planktonic state [4]. In order to control the respiratory tract bacterial infections, there are tremendous approaches and multiple treatments with a wide-range of drugs available which are quite expensive and producing some undesirable side effects [5, 6]. Therefore, there have been a growing interest toward metal-based NPs, which can be exhibiting the multi functionality of antibacterial activity [7, 8]. Among the metal-based NPs, the Ag or the combination of Ag/AgCl NPs has extensive role in biomedical and environmental applications [9, 10]. Moreover, very few researchers have reported that Ag/AgCl NPs can be prepared from different synthesis methods [11, 12].

In this global environment, there is a diverse range of organisms with special characteristic features. These organisms are the sources of different organic materials, which can be used to manipulate or engineer the suitable nanomaterials. PCU is one of the important constituents for the antimicrobial material in traditional medicine for the hundreds of years [13]. It is also encouraged as single or in combination with other drugs for medicinal uses. GC-MS analysis of PCU conferred the presence of 14 major volatile and non-volatile components such as phosphorus, nitrogen, chloride, potassium, calcium, urinary proteins, and hormones. It also confirmed the presence of 1-iodoundence and di-n-propyphalate which are only present during the pregnancy period [14] because of the prevention of microbial infections to its baby. It has been observed that there are some specific herbal compounds in PCU which are not digested by bacterial enzymes with high medicinal values. Such compounds are acting as a reducing factor or key molecules for the synthesis of metal-NPs and their coating could be seen on the surface of the prepared NPs. These NPs have strong antimicrobial effects. Since last decades, several novel methods were used in the development of nanomaterials that combined with other macromolecules to produce the hybrid nanomaterials against pathogenic microorganisms [15]. Amongst the macromolecules, the chitosan (c) has been widely used to coat the NPs. Chitosan is derived from the chitin biomolecules and it has biocompatible and ecofriendly nature with lower level of toxicity and antimicrobial property [16].

However, in our knowledge, no reports are available on the fabrication and characterizations of PCU@C-Ag/AgCl NPs along with its antimicrobial properties against RTI pathogens. In this context, owing of the present work focuses on the biosynthesis, structural, chemical, and elemental analysis of PCU@C-Ag/AgCl NPs and its antimicrobial potential against RTI bacteria and a fungal strain *Candia albicans*.

2 Materials and Methods

2.1 Chemicals

Silver nitrate ($AgNO_3$), Chitosan ($C_{56}H_{103}N_9O_{39}$) (Degree of deacetylation 70–90%, low molecular weight) and MTT (3-(4,5-dimethylthiazol-2-yl) 2,5-diphenyltetrazolium Bromide) were purchased from Hi Media, India.

2.2 Preparation of PCU sample

For the current examination, one liter of urine was gathered from the 5 years old individual pregnant cow after 60–75 days of the post-artificial insemination in urine bags. Following the urine collection, Phenylmethyl Sulfonyl Fluoride (PMSF, 0.01%) was added to degrade the proteins present in the urine and then urine was filtered by the Whatman Filter Paper (Grade No. 1, Size: 110 mm), and kept at − 20°C till further use.

2.3 Synthesis and purification of Ag/AgCl NPs

Ag/AgCl NPs have been synthesized by adding 2 mL of PCU sample (S1) to 1 mL of $AgNO_3$ solution (Stock − 30 mL) and the solution mixture was taken into 250 mL reaction vessel. The reaction vessel was subsequently shaken at 150 rpm in the dark condition on room temperature (RT). After 15 min, the reaction mixture was turned into the yellowish-brown color, which indicated the formation of Ag/AgCl NPs. The different volumes of PCU sample like 5, 8, 10, and 20 mL (S2, S3, S4, and S5) were used in the same procedure. After the completion of all the reactions, Ag/AgCl NPs were collected and centrifuged at 6000 rpm for 20 min. Then, the obtained pellet was rinsed with deionized H_2O (dH_2O) for few minutes and air-dried. The air-dried Ag/AgCl NPs were lyophilized and it was stored for further use.

2.4 Preparation of PCU@C-Ag/AgCl NPs

For the preparation of chitosan, 50 mg chitosan was added to 0.1 M acetic acid (20 mL) in a 100 mL conical flask. The

burette was filled with 20 mL of chitosan solution and was added drop by drop (3 mL/min) into the prepared PCU-Ag/AgCl reaction mixture. The reaction mixture was kept on the magnetic stirrer with optimum rotations for 25 min and it could lead to the formation of PCU@C-Ag/AgCl NPs. These NPs were purified with dH_2O and centrifuged at 5000 rpm for 15 min. The final purified NPs dried at RT to get the final product.

2.5 Physicochemical characterizations of PCU@C-Ag/AgCl NPs

The synthesized PCU@C-Ag/AgCl NPs were physicochemically characterized via different techniques. Like, the absorbance spectra of NPs were plotted by UV-Visible spectrophotometer (JASCO, USA) between 200 and 600 nm range. The crystalline structure of NPs was determined using XRD diffraction pattern. The size and shape of NPs was analyzed by Transmission Electron Microscopy (TEM) (Technai G2, at 200 kV). The elemental constitution of the PCU@C-Ag/AgCl NPs was determined through Energy Dispersive X-Ray spectroscopy (EDS). The functional groups of NPs were found out through the FT-IR spectroscopy (Shimadzu IR-Prestige-21).

2.6 Microbial cultures

The five RTI bacterial isolates were obtained from the PSG Institute of Medical Sciences and Research, Tamilnadu, India. These bacterial strains were as follows: *Pseudomonas aeruginosa*, *Klebsiella pneumoniae*, *Salmonella enteritidis*, *Staphylococcus aureus*, *Escherichia coli*, and *Seretia marcescens*. These bacterial cultures were stored at optimum conditions and sub-cultured prior to their use for biomedical applications. Also, the fungal strain *Candida albicans* (MTCC 227) purchased from Microbial Type Culture Collection (MTCC), Chandigarh, India. The fungal strain was cultured in the yeast peptone dextrose (YPD) for further applications.

2.7 Effect of PCU@C-Ag/AgCl NPs on RTI bacterial growth

To study the effects of PCU@C-Ag/AgCl NPs on bacterial growth, the following bacterial strains such as *P. aeruginosa*, *E. coli*, *S. aureus*, *S. marcescens*, *K. pneumoniae*, and *S. enteritidis* were cultured with different concentrations of NPs (5, 10, and 20 µg/mL) in the nutrient broth media

for 24 h at 37°C. Next, the bacterial growth was monitored and their absorbance was measured on different time intervals by UV/Visible spectrophotometer (JASCO, USA) at 600 nm. Using these absorbance values, the growth curves of treated bacterial strains were plotted.

2.8 Determination of MIC, MBC, and MFC values

The MIC values of PCU@C-Ag/AgCl NPs were calculated using the earlier reported method for different bacterial strains such as *K. pneumoniae*, *E. coli*, *P. aeruginosa*, *S. aureus*, *S. marcescens*, and *S. enteritidis* [17]. The different bacterial cultures were grown in Mueller–Hinton broth media at 37°C for 24 h and these cultures were diluted to 1.6×10^4 CFU/mL. Then, 200 µL culture of each bacterial strain were treated with different concentrations of NPs like 0.5, 1, 10, 20, 30, 40, and 50 µg/mL in a 96-well microplate. In addition, the untreated bacterial culture was kept as control during the experiment. The microplate was kept in an incubator for next 24 h and the optical densities of control and treated culture were measured at 550 nm using ELISA plate reader (Berthold Technologies, USA). Further, the Minimum Bactericidal Concentrations (MBC) of NPs in different bacterial cultures were also calculated. Next, the Minimum Fungicidal Concentration (MFC) of NPs was calculated against *C. albicans* using the earlier reported method [17].

2.9 Antibacterial Activity

The disc diffusion method was performed to study the antibacterial property of PCU@C-Ag/AgCl NPs against *S. aureus*, *K. pneumoniae*, *P. aeruginosa*, *S. enteritidis*, *S. marcescens*, and *E. coli*. The 1.6×10^4 CFU/mL of each bacterial culture was inoculated and spread out on the Mueller-Hinton agar plate and kept for 24 h at 37°C for incubation. Then, 5 mm sterile paper discs were inserted in the cultured bacterial plate and these discs were loaded with 10, 30, and 50 µg/mL of PCU@C-Ag/AgCl NPs. Further, the plates were incubated for next 24 h at 37°C and the antibacterial activity of NPs was examined by calculating the Zone of Inhibition (ZoI).

2.10 Antifungal activity

The antifungal property of PCU@C-Ag/AgCl NPs was determined by the mycelium growth inhibition test. The 20

µg/mL concentration of PCU@C-Ag/AgCl NPs was added into the potato dextrose agar medium. The *C. albicans* culture was poured into the center of petri dishes and plates were incubated for next 10 days at 28°C. The fungal growth was measured by calculating their mean radius. During the experiment, the untreated fungal culture was kept as negative control. The percentage of fungal growth inhibition was calculated using the following formula:

$$\text{Inhibition of mycelium (\%)}$$
$$= \left[\frac{\text{Growth of control} - \text{Growth of treatment}}{\text{Growth of control}} \right] \times 100$$

2.11 Bacterial cell morphology analysis

FESEM was used to examine the morphology of the bacterial cells treated with PCU@C-Ag/AgCl NPs along with untreated bacteria. In brief, *K. pneumoniae* and *S. enteritidis* bacterial culture were incubated with 50 µg/mL concentrations of NPs for 3h along with control. These cultures were grown on a sterile glass slide kept in a 24 well plate. Then, bacterial cells were washed with 0.85% NaCl solution and 2% glutaraldehyde was added to fix the bacterial cells at RT. After fixation, cells were washed with d.H_2O and 0.1 M PBS. Further, the cells were dehydrated in different percentages (70, 80, 90, and 100%) of ethanol for 10 min. In end, the bacterial cell morphology was examined by FESEM.

2.12 Statistical analysis

All the experimental results were analyzed and the graphs were plotted using Graph Pad Prism Software (GraphPad, USA). The experiments were carried out in triplicates (n = 3) and three independent times.

3 Results and Discussion

3.1 Preparation of PCU@C-Ag/AgCl NPs

In the present study, the Ag/AgCl NPs were synthesized using PCU sample. This formation of PCU-Ag/AgCl NPs was initially confirmed by the colour change of reaction mixture from pale yellow to dark brown color. The bioactive compounds present in PCU lead to the formation of Ag/AgCl NPs [19]. In our synthesis method, we did not use NaCl solution because it is enormously present in PCU sample. Thus, NaCl could react with silver nitrate ions and formed Ag/AgCl NPs after 24 h. In next step, chitosan so-

lution was added to the PCU-Ag/AgCl NP solution and a color change was seen from the dark brown to pale brown. This could lead to the formation of PCU@C-Ag/AgCl NPs. The similar results were also reported by Zondi Nate *et al*. They observed a color change during the synthesis of chitosan coated Ag NPs. They stated that the functional groups present in chitosan (OH, -NH_2) responsible for metal NPs synthesis because these groups possess strong attractions towards the metal ions that help in the binding of metals. Also, these groups act as capping agent and stabilise the NPs [20, 21].

3.2 Physicochemical characterizations of PCU@C-Ag/AgCl NPs

3.2.1 UV-Visible spectral analysis

The UV–Visible spectral analysis of PCU@C-Ag/AgCl NPs is shown in Figure 1. We observed a highest absorption peak or surface plasmon resonance (SPR) peak for Ag NPs at 420 nm [22]. When we added 2 to 20 mL volumes of PCU in $AgNO_3$ solution then we found a steady increase in the absorbance values of PCU@C-Ag/AgCl NPs without any change in their highest peak position till 24 h of reaction time. The absorbance spectrum of PCU@C-Ag/AgCl NPs gradually increased by increasing the concentration of reaction mixture, which indicated the maximum fabrication of PCU@C-Ag/AgCl NPs. It was likely achieved at the larger volume/concentration of PCU (20 mL) after mixing the precursor solution of $AgNO_3$ [23]. Next, the higher concentration of PCU@C-Ag/AgCl NPs was used for further physicochemical characterization analysis. The obtained
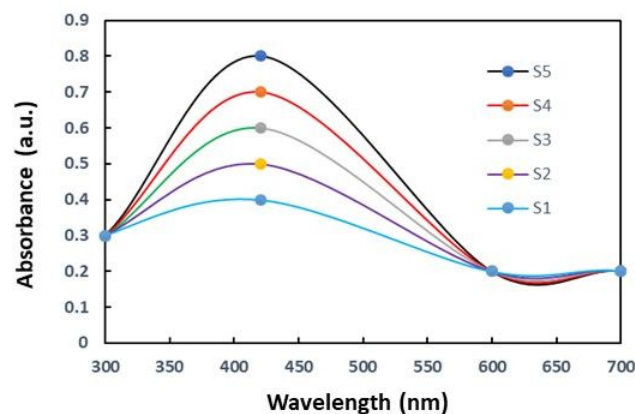

Figure 1: UV–Visible absorption spectra of PCU@C-Ag/AgCl NPs synthesized using S1 (2 mL), S2 (5 mL), S3 (8 mL), S4 (10 mL), and S5 (20 mL) of PCU

UV-Visible spectrum showed that high concentration of PCU sample was required to reduce Ag^+ to Ag^0.

3.2.2 FT-IR spectral analysis

The functional group analysis was carried out by FTIR spectroscopy as shown in Figure 2. We identified the possible chemical interactions between the bioactive molecules present in PCU sample and Ag/AgCl NPs. We observed several vibrational peaks for different functional groups which were indicated as O-H group stretching peak at 3348.42 cm^{-1}, C-H stretching peak at 2831.30 cm^{-1} and 2360.87 cm^{-1}, C≡C stretching peak at 2121.70 cm^{-1}, and C-C stretching peak at 1635.64 cm^{-1} in the FTIR spectrum of PCU sample. Similarly, the FTIR spectrum of PCU@C-Ag/AgCl NPs displayed multiple vibrational peaks at 3865.35 cm^{-1}, 3741.90 cm^{-1} and 3329.79 cm^{-1} for O-H group which were not seen after the reduction of Ag^+. The hydroxyl group reduction could indicate the formation of Ag^0 NPs from Ag^+ ions [24]. The FTIR results suggest that different functional groups such as O-H, C-H, C≡C, C-C, N-H exists in the PCU due to the presence of various bioactive compounds such as cresol, lactose, urea, uric acids, and polysaccharides. These compounds play an important role in Ag^+ to Ag^0 reduction, and act as capping agents to stabilize the prepared Ag/AgCl NPs. The intense peak at 2322.29 cm^{-1} exhibited the presence of C-H stretching of aldehyde group and the peak at 1512.19 cm^{-1} showed the N-H stretching of polysaccharides. This indicated the presence of chitosan [25]. The vibrational peaks at 686.66 cm^{-1}, 601.79 cm^{-1}, and 563.21 cm^{-1} correspond the presence of C-Br and C-H groups. This indicated the presence of alkyl halides and alkynes respec-
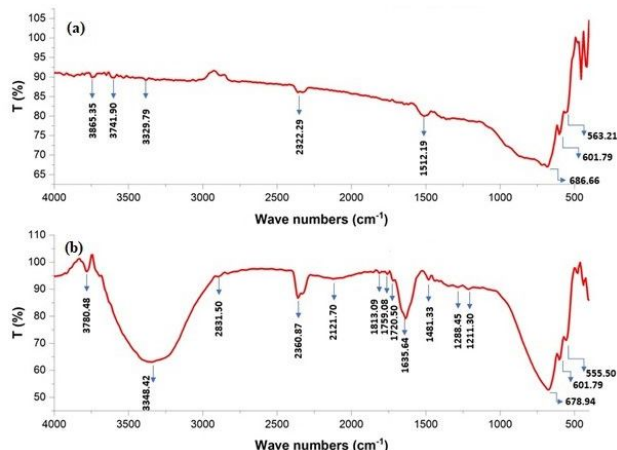
tively. This experiment could indicate the binding efficiency of different bioactive compounds present in PCU sample and acted as reducing agents to form Ag/AgCl NPs.

3.2.3 XRD analysis

The phase purity of PCU@C-Ag/AgCl NPs powder was studied by X-ray diffraction technique. We observed 10 distinct diffraction peaks such as 27.8°, 32.2°, 38.2°, 46.2° (220), 54.8°, 57.5°, 64.7°, 67.4°, 74.2°, and 76.4° at 2θ angle in the XRD pattern (Figure 3) which corresponds to the different orientation planes (111), (200), (220), (311), (222), (400), (311), and (420) of AgCl NPs (Standard JCPDS no. 85-1355). Also, some lower peaks were seen at 38.2° and 64.7° at 2θ angle which indicated the cubic phase of Ag NPs (JCPDS no. 65-2871). The XRD analysis showed the crystalline and face-centered cubic (FCC) configuration of PCU@C-Ag/AgCl NPs. These results were also documented by other researchers [26–28]. The average crystalline size of PCU@C-Ag/AgCl NPs was calculated by the Scherrer equation and it was calculated to be 49.58 nm [29].
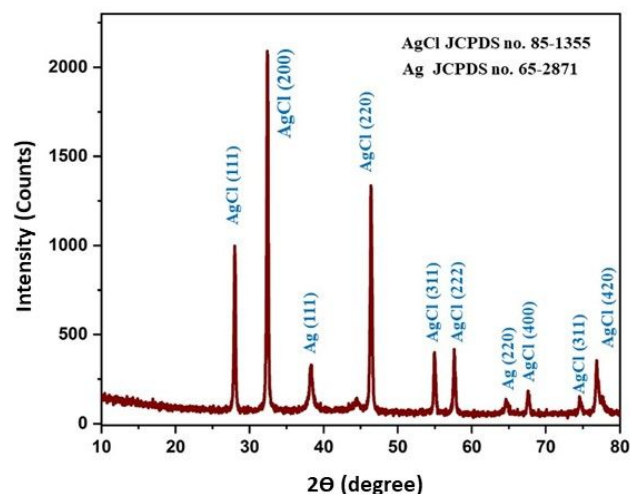

Figure 3: XRD pattern analysis of PCU@C-Ag/AgCl NPs. The diffractions planes of NPs were interpreted with JCPDS file indicating their FCC configuration

3.2.4 EDS analysis

The elemental composition of PCU@C-Ag/AgCl NPs was analyzed using EDS. The EDS spectrum displayed a strong peak around 3.29 keV which corresponds to the binding energy of Ag ions. We also confirmed the PCU@C-Ag/AgCl
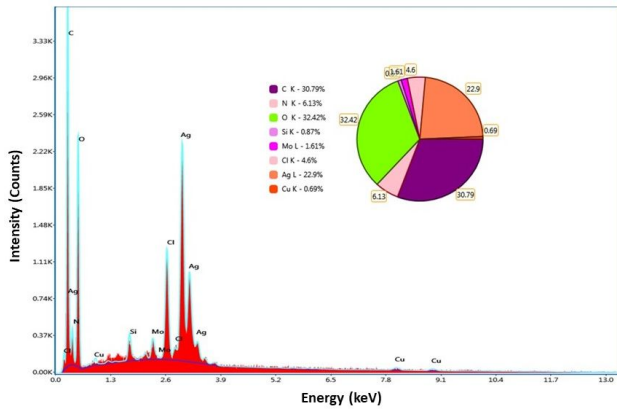

Figure 2: FTIR analysis of (a) PCU@C-Ag/AgCl NPs, and (b) PCU sample ranging between 500–4000 cm^{-1}

Figure 4: EDS analysis of PCU@C-Ag/AgCl NPs. In the spectrum, a strong peak for Ag confirmed the stability and purity of PCU@C-Ag/AgCl NPs

NPs formation and observed their prime elemental composition such as carbon (30.79%), oxygen (32.42%), silicone (0.87%), (Molybdenum (1.61%), and silver (22.9%). Besides it, an intense peak for Ag was found 3.0 keV and for Cl (4.6%) at 2.6 and 2.7 keV. The intense peaks of Ag and Cl revealed the Ag/AgCl NPs formation (Figure 4). These results were supported with the previous data where several biological sources were used for the formation Ag/AgCl NPs [30, 31]. Similarly, the EDS spectrum of PCU@C-Ag/AgCl NPs exhibited a peak for nitrogen (6.13%) due to the excitation of X-ray from chitosan. This confirmed the presence of the amine (-NH$_2$) group [32].

3.2.5 TEM imaging of PCU@C-Ag/AgCl NPs

TEM image showed the uniform size and almost spherical shape of PCU@C-Ag/AgCl NPs with less agglomeration (Figure 5). The particle size range was between 2.17 and 32.28 nm. The particle agglomeration could be prevented due to the chemical constituents of PCU [33].
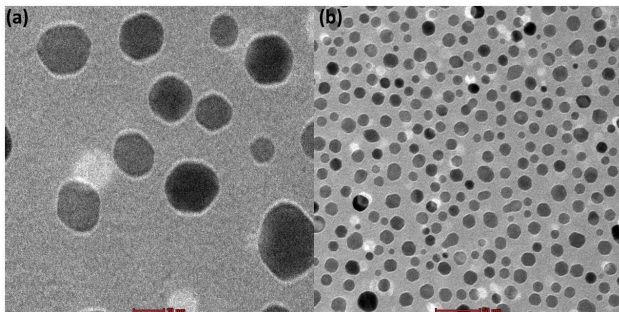

Figure 5: TEM imaging of PCU@C-Ag/AgCl NPs (a) high and (b) low magnifications

3.3 Effect of PCU@C-Ag/AgCl NPs on RTI bacterial growth

The inhibitory effect of PCU@C-Ag/AgCl NPs on RTI bacterial pathogen's growth showed in Figure 6. We observed the growth of all tested bacterial pathogens at lowest concentration of NPs (5 µg/mL) which was relatively below the growth curve of control. Moreover, the 10 and 20 µg/mL concentrations of NPs inhibited the growth of all tested bacterial pathogens. Thus, these results could display the potent antibacterial activity of PCU@C-Ag/AgCl NPs.

3.4 Determination of MIC, MBC, and MFC values

The antimicrobial activities of PCU@C-Ag/AgCl NPs were analyzed for different bacterial strains and *C. albicans* fungi by calculating their MIC values as shown in Table 1. As, MBC and MFC values are the lowest concentrations of any antimicrobial agent that kill the microorganisms. These values were also calculated and shown in Table 1. Conclusively, the tabular data represented the potent antimicrobial activity of PCU@C-Ag/AgCl NPs against RTI pathogens.

Table 1: MIC, MBC, and MFC values of PCU@C-Ag/AgCl NPs against tested RTI bacterial pathogens and *C. albicans* fungi

Bacterial/Fungal samples	MIC (µg/mL)	MBC/MFC (µg/mL)
K. pneumoniae	2.6	2.4
P. aeruginosa	2.5	2.0
S. enteritidis	2.3	2.2
E. coli	4.3	3.8
S. aureus	3.9	3.6
S. marcescens	4.1	3.4
C. albicans	4.5	4.4

3.5 Antibacterial activity

The antibacterial activity of PCU@C-Ag/AgCl NPs were studied against RTI bacterial pathogens and measured their ZoI as shown in Figure 7. We observed the clear ZoI in *K. pneumoniae* culture and their values were calculated to be 12.7 and 23 mm for the 10 and 20 µg/mL concentrations of NPs respectively. Similarly, the ZoI values in *S. enteritidis culture* were calculated to be 4.2, 7.3, and 18.5 mm for 5, 10, and 20 µg/mL concentrations of NPs respectively. The minimum
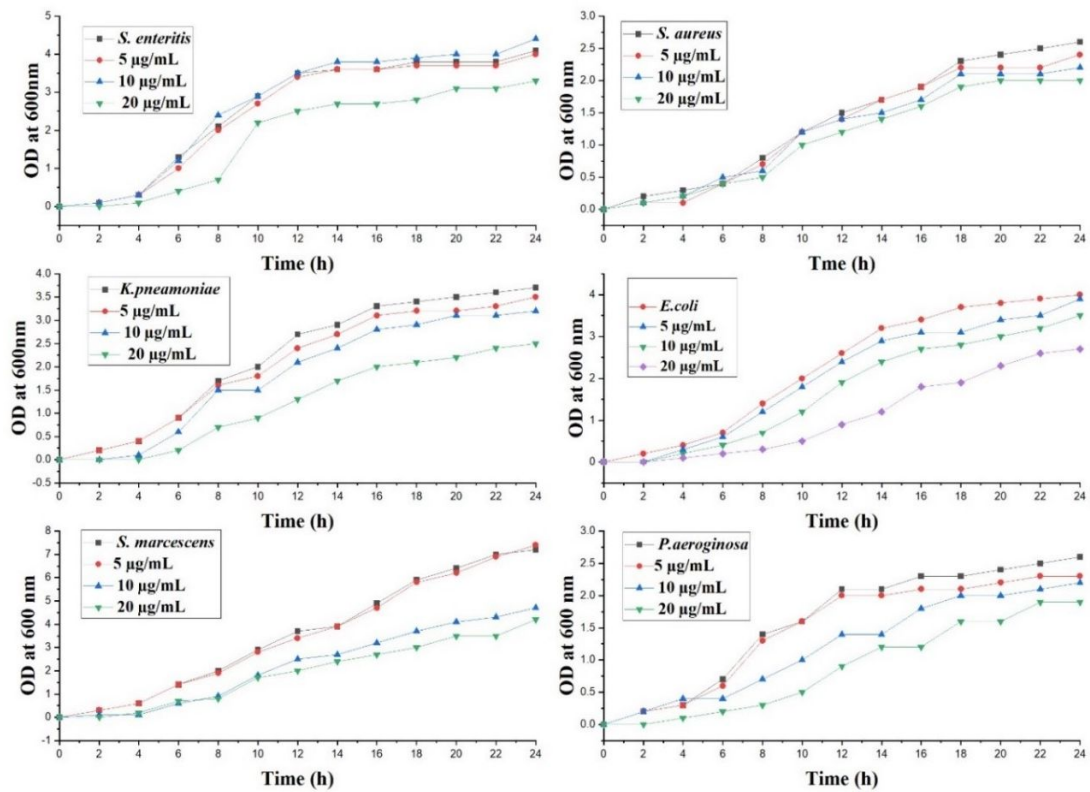
Figure 6: The growth curve of RTI bacterial pathogens treated with 5, 10, and 20 µg/mL concentrations of PCU@C-Ag/AgCl NPs
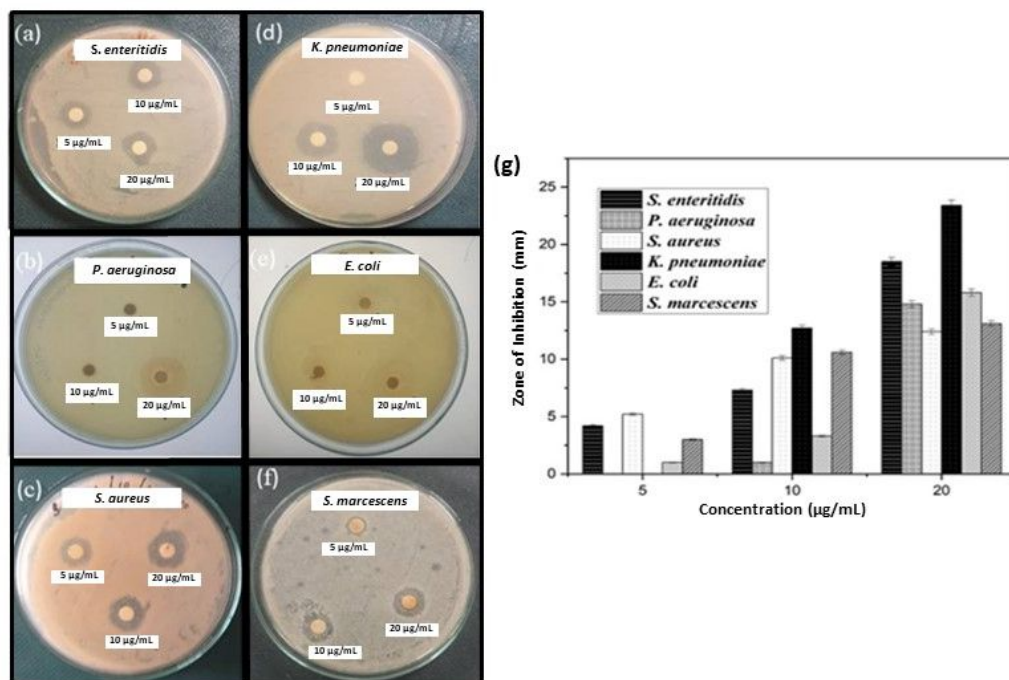

Figure 7: Antibacterial activity of PCU@C-Ag/AgCl NPs (a – f) analysed by calculating ZoI in different RTI bacterial pathogen's culture. The ZoI is measured in mm and their values are represented in the histogram (n = 3) (g)

ZoI was calculated to be 3 mm in *S. marcescens* culture for 5 µg/mL concentration of NPs. Further, the *P. aeruginosa* culture was found to be more sensitive for 10 and 20 µg/mL concentrations of NPs. Hence, we observed an increase in ZoI values on dose-dependent manner. Based on the ZoI data, we showed the strong antibacterial activity against selected RTI bacterial pathogens in the following order: *K. pneumoniae* > *S. enteritidis* > *P. aeruginosa* > *S. marcescens* > *S. aureus* > *E. coli*.

In previous studies, the cow urine has been proven for strong antibacterial activity [34, 35]. The presence of various bioactive compounds in PCU exhibited potent antibacterial activity [36, 37]. The Ag NPs synthesized using cow urine, have been found to be bactericidal nature [38]. However, none of the study used PCU for fabricating Ag NPs. Thus, our study first-time reports the synthesis of PCU@C-Ag/AgCl NPs and display their antibacterial role against RTI bacterial pathogens.

3.6 Antifungal activity

The antifungal effect of PCU@C-Ag/AgCl NPs was carried out on the mycelial growth culture of *C. albicans* till 14th day of incubation as shown in Figure 8. We observed a reduction in the radial growth of fungal mycelium till 14th day of incubation period. We did not observe any growth in-hibition in control plate. We treated the *C. albicans* culture with 20 µg/mL concentration of PCU@C-Ag/AgCl NPs at 0 day and we found 0.7 cm mycelium growth at 2nd day in treated fungal culture but in control, the mycelium growth was 3.4 cm. Following the 7th day, the mycelium growth in treated culture was calculated to be 0.87 cm but the control showed a steady growth (17 cm). After the end of 14th day, the NPs treated culture exhibited the medium level growth (15.4 cm) while in control, the culture plate showed the full growth of *C. albicans* (47.8 cm).

In last two decades, the silver-based nanomaterials have been used to inhibit and kill the fungal pathogens [39]. In 2016, Ding *et al.*, reported that the growth of *C. albicans* inhibited due to the endogenous ROS (Reactive Oxygen Species) leading to the oxidative damage in fungal cells [40]. The metal ions released by NPs causes disturbed electron-shuttling process, membrane structure disruption, cellular enzyme deactivation, depleted redox potential levels, and reduced mitochondria membrane potentials thus inducing the accumulation of ROS inside the cells. This ROS production can be also strongly associated with both size and shape of NPs [41–48]. Further, the transcriptome analysis revealed that Ag NPs damage the fungal cell by denaturing the transmembrane protein [49]. In our study, the mycelial growth of *C. albicans* inhibited due to ROS production and cell wall damage.
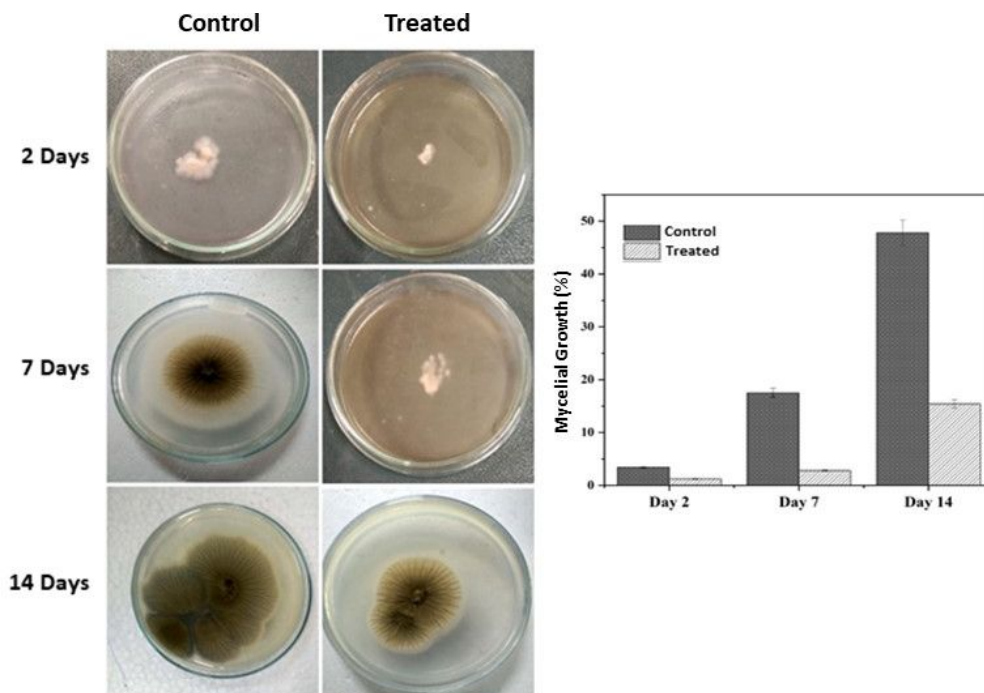

Figure 8: Antifungal activity of PCU@C-Ag/AgCl NPs on the radial mycelial growth of *C. albicans*. The images of control and treated fungal culture were taken on 2nd, 7th and 14th day. The percentage of mycelial growth was plotted in a histogram
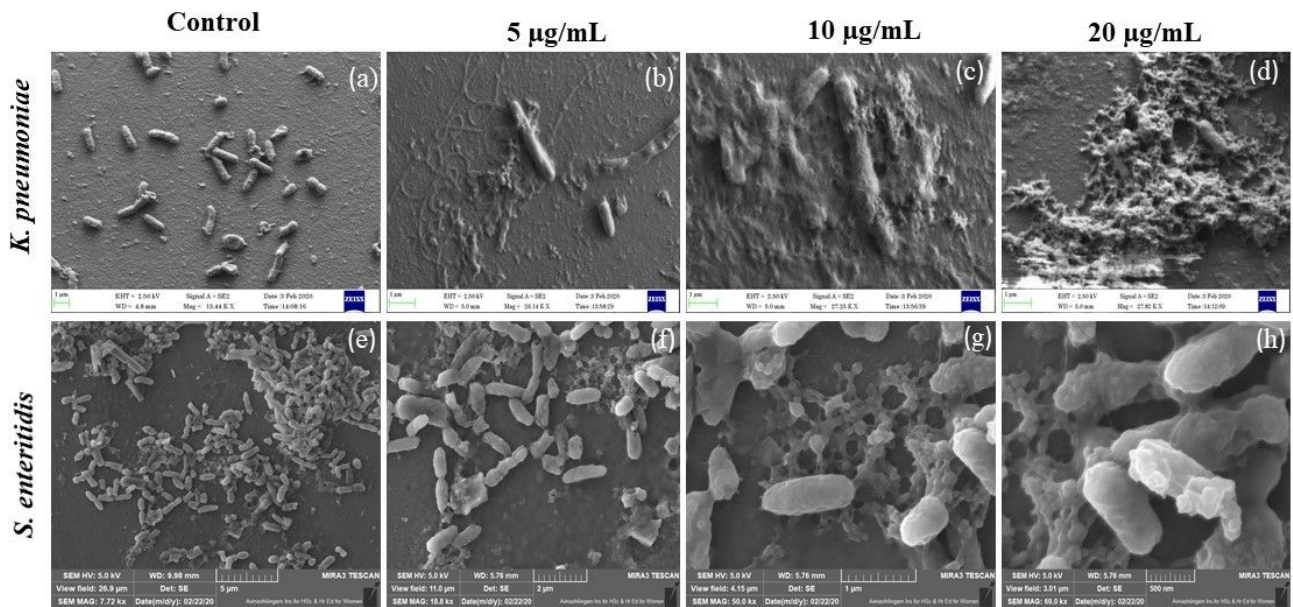
Figure 9: The bacterial cell morphological analysis by FESEM for both untreated and PCU@C-Ag/AgCl NPs treated *K. pneumoniae* and *S. enteritidis* bacteria. The damages and cell lysis observed in the bacteria. The scale bar corresponds to 1, 2, and 5 μm

3.7 FESEM analysis of PCU@C-Ag/AgCl NPs treated bacterial cell morphology

The bacterial cell morphology was studied by FESEM analysis for both untreated and PCU@C-Ag/AgCl NPs treated *K. pneumoniae* and *S. enteritidis* bacteria (Figure 9). We observed several changes and damages in the cell morphology of treated bacteria which may be due to the binding of NPs on the surface of the bacteria. These changes were seen in bacterial cell wall and membrane [50–52]. However, no morphological changes were seen in untreated bacteria.

4 Conclusions

The development of new drugs is always preferred for the treatment of respiratory tract infections caused by drug resistant bacteria. Also, the fabrication of low cost, ecofriendly, and biocompatible materials required as an alternative to treat such drug resistant bacterial pathogens. In this study, we first-time synthesized the chitosan coated Ag/AgCl NPs using PCU sample which contains various bioactive compounds that act as reducing and capping agents for the synthesis of the NPs. These NPs were crystalline in nature and found to be almost spherical in shape with a particle size range between 2.17 nm to 32.28 nm. Also, these NPs were used as antimicrobial material against RTI pathogens. Conclusively, this novel nanomaterial may be tested for respiratory tract infections in clinics.

Author's Contribution: S.P. – Writing – Original draft, Conceptualization, Visualization; K.S. – Writing - Original draft; L.G.B. – Writing - Review & Editing; J.A. – Writing - Review & Editing; A.G. – Writing - Review & Editing; S.B. – Writing - Review & Editing; R.R. – Writing - Review & Editing; N.K.J. – Writing - Review & Editing; S.P. – Writing - Review & Editing; S.K.S. – Writing - Review & Editing; K.D. – Writing - Review & Editing; P.K.G. – Conceptualization, Visualization, Project administration

Conflict of interests: The authors declare no conflict of interest.

Ethical approval: The conducted research is not related to either human or animal use.

Data availability statement: The datasets generated during and/or analysed during the current study are available from the corresponding author on reasonable request.

References

[1] Forum of International Respiratory Societies. The Global Impact of Respiratory Disease. 2nd ed. Sheffield: European Respiratory Society; 2017.

[2] Rudan I, Boschi-Pinto C, Biloglav Z, Mulholland K, Campbell H. Epidemiology and etiology of childhood pneumonia. Bull World Health Organ. 2008 May;86(5):408–16.

[3] Donlan RM, Costerton JW. Biofilms: survival mechanisms of clinically relevant microorganisms. Clin Microbiol Rev. 2002 Apr;15(2):167–93.

[4] Lewis K. Multidrug tolerance of biofilms and persister cells. Bacterial biofilms. 2008, 107-131. https://doi.org/10.1007/978-3-540-75418-3_6.

[5] Nikaido H. Multidrug resistance in bacteria. Annu Rev Biochem. 2009;78(1):119–46.

[6] Ding X, Duan S, Ding X, Liu R, Xu FJ. Versatile antibacterial materials: an emerging arsenal for combatting bacterial pathogens. Adv Funct Mater. 2018;28(40):1802140.

[7] Ansari MA, Alzohairy MA. One-pot facile green synthesis of silver nanoparticles using seed extract of Phoenix dactylifera and their bactericidal potential against MRSA. Evid Based Complement Alternat Med. 2018 Jun;2018:1860280.

[8] Senthilkumar P, Kumar DR, Sudhagar B, Vanthana M, Parveen MH, Sarathkumar S, et al. Seagrass-mediated silver nanoparticles synthesis by Enhalus acoroides and its α-glucosidase inhibitory activity from the Gulf of Mannar. J Nanostructure Chem. 2016;6(3):275–80.

[9] Gawali P, Jadhav BL. Synthesis of Ag/AgCl Nanoparticles and their action on Human Serum albumin: A fluorescence study. Process Biochem. 2018;69:106–22.

[10] Okaiyeto K, Ojemaye MO, Hoppe H, Mabinya LV, Okoh AI. Phytofabrication of silver/silver chloride nanoparticles using aqueous leaf extract of Oedera genistifolia: characterization and antibacterial potential. Molecules. 2019 Nov;24(23):4382.

[11] Alishah H, Pourseyedi S, Mahani SE, Ebrahimipour SY. Extract-mediated synthesis of Ag@ AgCl nanoparticles using Conium maculatum seeds: characterization, antibacterial activity and cytotoxicity effect against MCF-7 cell line. RSC Advances. 2016;6(77):73197–202.

[12] Al Aboody MS. Silver/silver chloride (Ag/AgCl) nanoparticles synthesized from Azadirachta indica lalex and its antibiofilm activity against fluconazole resistant Candida tropicalis. Artif Cells Nanomed Biotechnol. 2019 Dec;47(1):2107–13.

[13] Fulendra S, Senthil KM, Mahadevan N. Nutraceuticals: uplift in health. Int. J. Recent. Adv. Pharm Res. 2012;2(2):17–28.

[14] Kumar KR, Archunan G, Jeyaraman R, Narasimhan S. Chemical characterization of bovine urine with special reference to oestrus. Vet Res Commun. 2000 Nov;24(7):445–54.

[15] Rivero PJ, Urrutia A, Goicoechea J, Zamarreño CR, Arregui FJ, Matías IR. An antibacterial coating based on a polymer/sol-gel hybrid matrix loaded with silver nanoparticles. Nanoscale Res Lett. 2011 Apr;6(1):305.

[16] Verlee A, Mincke S, Stevens CV. Recent developments in antibacterial and antifungal chitosan and its derivatives. Carbohydr Polym. 2017 May;164:268–83.

[17] Wayne P. Performance standard for antimicrobial susceptibility testing. Clinical and laboratory standards institute (CLSI). 26th informational supplement. 2016, 33(1), M100-S23.

[18] Kim SW, Jung JH, Lamsal K, Kim YS, Min JS, Lee YS. Antifungal effects of silver nanoparticles (AgNPs) against various plant pathogenic fungi. Mycobiology. 2012 Mar;40(1):53–8.

[19] Jain NK, Gupta VB, Garg R, Silawat N. Efficacy of cow urine therapy on various cancer patients in Mandsaur District, India-A survey. International Journal of Green Pharmacy. 2010;4(1):29.

[20] Nate Z, Moloto MJ, Mubiayi PK, Sibiya PN. Green synthesis of chitosan capped silver nanoparticles and their antimicrobial activity. MRS Adv. 2018;3(42):2505–17.

[21] Jayakumar R, Menon D, Manzoor K, Nair SV, Tamura H. Biomedical applications of chitin and chitosan-based nanomaterials-A short review. Carbohydr Polym. 2010;82(2):227–32.

[22] Sharma G, Nam JS, Sharma AR, Lee SS. Antimicrobial potential of silver nanoparticles synthesized using medicinal herb coptidis rhizome. Molecules. 2018;23(9):2268.

[23] Sharifi-Rad M, Pohl P, Epifano F. Phytofabrication of Silver Nanoparticles (AgNPs) with Pharmaceutical Capabilities Using Otostegia persica (Burm.) Boiss. Leaf Extract. Nanomaterials. 2021,11,1045. https://doi.org/https://doi.org/10.3390/nano.11041045.

[24] Iravani S, Korbekandi H, Mirmohammadi SV, Zolfaghari B. Synthesis of silver nanoparticles: chemical, physical and biological methods. Res Pharm Sci. 2014 Nov-Dec;9(6):385–406.

[25] Qi L, Xu Z, Jiang X, Hu C, Zou X. Preparation and antibacterial activity of chitosan nanoparticles. Carbohydr Res. 2004 Nov;339(16):2693–700.

[26] Han C, Ge L, Chen C, Li Y, Zhao Z, Xiao X, et al. Site-selected synthesis of novel Ag@ AgCl nanoframes with efficient visible light induced photocatalytic activity. J Mater Chem A Mater Energy Sustain. 2014;2(31):12594–600.

[27] Plotnichenko VG, Philippovskiy DV, Sokolov VO, Golovanov VF, Polyakova GV, Lisitsky IS, et al. Infrared luminescence in bismuth-doped AgCl crystals. Opt Lett. 2013 Aug;38(16):2965–8.

[28] Sun Y. Silver nanowires—unique templates for functional nanostructures. Nanoscale. 2010 Sep;2(9):1626–42.

[29] Senthilkumar P, Yaswant G, Kavitha S, Chandramohan E, Kowsalya G, Vijay R, et al. Preparation and characterization of hybrid chitosan-silver nanoparticles (Chi-Ag NPs); A potential antibacterial agent. Int J Biol Macromol. 2019 Dec;141:290–8.

[30] Okaiyeto K, Ojemaye MO, Hoppe H, Mabinya LV, Okoh AI. Phytofabrication of silver/silver chloride nanoparticles using aqueous leaf extract of Oedera genistifolia: characterization and antibacterial potential. Molecules. 2019 Nov;24(23):4382.

[31] Devi TB, Ahmaruzzaman M. Bio-inspired sustainable and green synthesis of plasmonic Ag/AgCl nanoparticles for enhanced degradation of organic compound from aqueous phase. Environ Sci Pollut Res Int. 2016 Sep;23(17):17702–14.

[32] Dananjaya SH, Kumar RS, Yang M, Nikapitiya C, Lee J, De Zoysa M. Synthesis, characterization of ZnO-chitosan nanocomposites and evaluation of its antifungal activity against pathogenic

Candida albicans. Int J Biol Macromol. 2018 Mar;108:1281–8.

[33] Alameen AO, Abdelatif AM. Metabolic and endocrine responses of crossbred dairy cows in relation to pregnancy and season under tropical conditions. Am-Eurasian J Agric Environ Sci. 2012;12(8):1065–74.

[34] Achliya GS, Meghre VS, Wadodkar SG, Dorle AK. Antimicrobial activity of different fractions of cow urine. Indian J. Nat. Prod. 2004;20:14–6.

[35] Raad S, Deshmukh DV, Harke SN, Kachole MS. Antibacterial activity of cow urine against some pathogenic and non-pathogenic bacteria. Int J Pharm Sci Res. 2018;4(4):1534.

[36] Mohanty I, Senapati MR, Jena D, Palai S. Diversified uses of cow urine. Int J Pharm Pharm Sci. 2014;6(3):20–2.

[37] Badadani M, SureshBabu SV, Shetty KT. Optimum conditions of autoclaving for hydrolysis of proteins and urinary peptides of prolyl and hydroxyprolyl residues and HPLC analysis. J Chromatogr B Analyt Technol Biomed Life Sci. 2007 Mar;847(2):267–74.

[38] Kim JH. Nano silver chemotherapeutic agents and its applications. News Inf. Chem. Eng. 2004;22:655–60.

[39] Niazi JH, Sang BI, Kim YS, Gu MB. Global gene response in Saccharomyces cerevisiae exposed to silver nanoparticles. Appl Biochem Biotechnol. 2011 Aug;164(8):1278–91.

[40] Ding Y, Li Z, Li Y, Lu C, Wang H, Shen Y, *et al.* HSAF-induced antifungal effects in Candida albicans through ROS-mediated apoptosis. RSC Advances. 2016;6(37):30895–904.

[41] Holt KB, Bard AJ. Interaction of silver(I) ions with the respiratory chain of Escherichia coli: an electrochemical and scanning electrochemical microscopy study of the antimicrobial mechanism of micromolar Ag+. Biochemistry. 2005 Oct;44(39):13214–23.

[42] Carlson C, Hussain SM, Schrand AM, Braydich-Stolle LK, Hess KL, Jones RL, *et al.* Unique cellular interaction of silver nanoparticles: size-dependent generation of reactive oxygen species. J Phys Chem B. 2008 Oct;112(43):13608–19.

[43] Jiang W, Kim BY, Rutka JT, Chan WC. Nanoparticle-mediated cellular response is size-dependent. Nat Nanotechnol. 2008 Mar;3(3):145–50.

[44] AshaRani PV, Low Kah Mun G, Hande MP, Valiyaveettil S. Cytotoxicity and genotoxicity of silver nanoparticles in human cells. ACS Nano. 2009 Feb;3(2):279–90.

[45] Zhang Y, Gu AZ, Xie S, Li X, Cen T, Li D, *et al.* Nano-metal oxides induce antimicrobial resistance via radical-mediated mutagenesis. Environ Int. 2018 Dec;121(Pt 2):1162–71.

[46] Zhang L, Wu L, Si Y, Shu K. Size-dependent cytotoxicity of silver nanoparticles to Azotobacter vinelandii: growth inhibition, cell injury, oxidative stress and internalization. PLoS One. 2018 Dec;13(12):e0209020.

[47] Huang T, Holden JA, Heath DE, O'Brien-Simpson NM, O'Connor AJ. Engineering highly effective antimicrobial selenium nanoparticles through control of particle size. Nanoscale. 2019 Aug;11(31):14937–51.

[48] Yu Z, Li Q, Wang J, Yu Y, Wang Y, Zhou Q, *et al.* Reactive Oxygen Species-Related Nanoparticle Toxicity in the Biomedical Field. Nanoscale Res Lett. 2020 May;15(1):115.

[49] Kumar NI, Das SA, Jyoti AN, Kaushik SA. Synergistic effect of silver nanoparticles with doxycycline against Klebsiella pneumoniae. Int J Pharm Pharm Sci. 2016;8(7):183–6.

[50] Rajawat S, Qureshi MS. Comparative study on bactericidal effect of silver nanoparticles, synthesized using green technology, in combination with antibiotics on Salmonella typhi. J Biomater Nanobiotechnol. 2012;3(4):480–5.

[51] Ahmed S, Ahmad M, Swami BL, Ikram S. A review on plants extract mediated synthesis of silver nanoparticles for antimicrobial applications: A green expertise. J Adv Res. 2016 Jan;7(1):17–28.

[52] Arora S, Jain J, Rajwade JM, Paknikar KM. Cellular responses induced by silver nanoparticles: in vitro studies. Toxicol Lett. 2008 Jun;179(2):93–100.